Accepted Manuscript

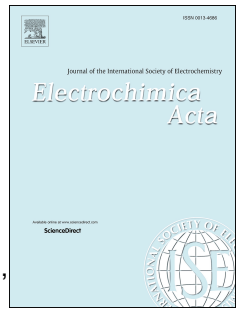

Design and modelling of a photo-electrochemical transduction system based on solubilized photosynthetic reaction centres

F. Milano, F. Ciriaco, M. Trotta, D. Chirizzi, V. De Leo, A. Agostiano, L. Valli, L. Giotta, M.R. Guascito

PII: S0013-4686(18)32207-2

DOI: 10.1016/j.electacta.2018.09.198

Reference: EA 32789

To appear in: *Electrochimica Acta*

Received Date: 3 May 2018

Revised Date: 28 September 2018

Accepted Date: 29 September 2018

Please cite this article as: F. Milano, F. Ciriaco, M. Trotta, D. Chirizzi, V. De Leo, A. Agostiano, L. Valli, L. Giotta, M.R. Guascito, Design and modelling of a photo-electrochemical transduction system based on solubilized photosynthetic reaction centres, *Electrochimica Acta* (2018), doi: https://doi.org/10.1016/j.electacta.2018.09.198.

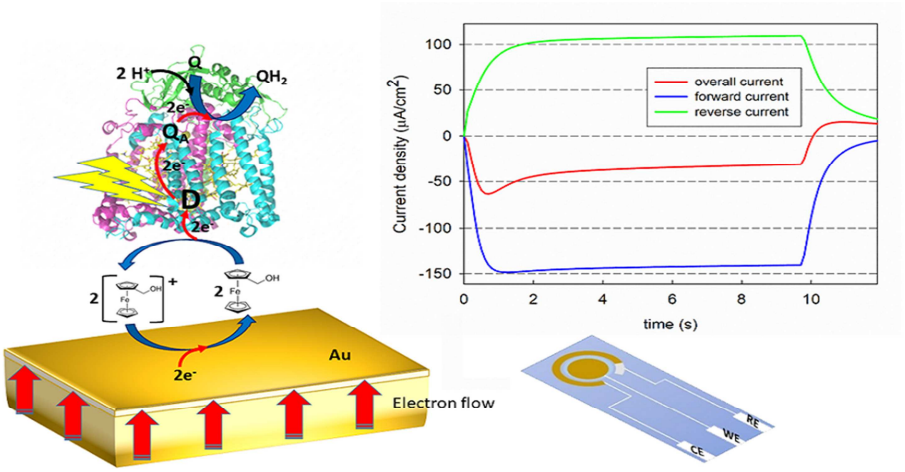

Design and modelling of a photo-electrochemical transduction system based on solubilized photosynthetic reaction centres

F. Milano[1], F. Ciriaco[2], M. Trotta[1], D. Chirizzi[3], V. De Leo[1,2], A. Agostiano[1,2], L. Valli[4], L. Giotta[4,*], and M. R. Guascito[4]

[1] CNR-IPCF Istituto per i Processi Chimico-Fisici, UOS Bari, Via Orabona 4, I-70125 Bari, Italy

[2] Dipartimento di Chimica, Università di Bari, Via Orabona 4, I-70125 Bari, Italy

[3] Istituto Zooprofilattico Sperimentale di Puglia e Basilicata, Via Manfredonia 20, I-71121 Foggia, Italy

[4] Dipartimento di Scienze e Tecnologie Biologiche ed Ambientali, Università del Salento & UdR INSTM di Lecce, c/o Campus Ecotekne, Via Monteroni, 73100 Lecce, Italy

[*] Corresponding author: livia.giotta@unisalento.it

Abstract

The bacterial photosynthetic reaction centre (RC) is a membrane spanning protein that, upon illumination, promotes the reduction of a ubiquinone molecule withdrawing electrons from cytochrome c_2. This photo-activated reaction has been often exploited, in suitably designed photoelectrochemical cells, to generate photocurrents sustained by the reduction at the working electrode of the photo-oxidised electron donor or by the oxidation of the electron acceptor. In this work we have explored in more detail the factors affecting the photocurrent generation in commercially available screen-printed electrochemical cells containing an electrolyte solution where RC proteins and suitable mediators are solubilized. In particular, the role of the applied potential and the influence of concentration and structure of acceptor

and donor molecules have been assessed. We show that efficient generation of cathodic photocurrents in a three electrode configuration occurs at an applied potential of 0.0 V *versus* quasi-ref Ag (the open circuit potential of the system measured in the dark) in presence of ferrocenemethanol and decylubiquinone, which proved to guarantee high performances as electron donor and acceptor respectively. Moreover, we employed a set of differential equations, describing reaction and diffusion processes, for modelling with high accuracy the chronoamperometry profiles recorded at variable RC concentrations. This model allowed us to estimate the kinetic parameters relevant to the chemical and electrochemical reactions triggered by light and to get a snapshot of the electrolyte composition in the bulk and electrode surroundings at different times from the light exposure. The characteristic time course of the photocurrent, showing a fast rise to a peak value followed by a slower decay, has been therefore explained as the result of the strict interconnection between the dynamical processes involved.

Keywords: photosynthetic reaction centre, *Rhodobacter sphaeroides*, quinone, photoelectrochemical cell, photocurrent, screen-printed electrode, photocycle, redox mediators.

1 Introduction

The reaction centre (RC) from the photosynthetic bacterium *Rhodobacter sphaeroides* is a membrane-spanning specialized pigment-protein complex where the primary processes of photosynthesis take place. This protein is relatively simple to isolate and sufficiently stable to allow its employment in photovoltaics or biosensing applications [1-4].

The protein has a weight of 100 kDa and consists of three subunits called H, L and M. Eight cofactors are non-covalently bound to the protein scaffold: a dimer (D) of bacteriochlorophylls (BChl) which acts as the primary electron donor, two accessory BChl,

two bacteriopheophytins (BPh) and two ubiquinones-10 (UQ_{10}). A non-heme Fe^{2+} is bound covalently to four histidine and one glutamate residues of the L and M protein chains. All cofactors are arranged in two symmetrical branches called A and B. As a consequence of light absorption, one electron is transferred from the singlet excited state of D, through the series of cofactors, to the UQ_{10} located in the A-branch pocket (Q_A) and finally to the ubiquinone in the B-branch pocket (Q_B). In vivo, the protein performs a photocycle in which the absorption of two photons triggers the reduction of the UQ_{10} sitting in Q_B to ubiquinol in a two-step fashion with the simultaneous oxidation of two cytochrome proteins and the uptake of two protons. The RC can be isolated from readily available bacterial biomass and is particularly stable against denaturation, which makes this protein advantageous compared with photosynthetic material extracted from plants [5]. Therefore, it is suitable for use in photoelectrochemical cells (PECs) to promote the conversion of visible light energy into electrical energy.

A number of PECs employing the bacterial RC as photoactive component have been developed in the last decade [6]. Much effort has been devoted to the optimization of protein/electrode electrical communication by suitable protein immobilization strategies [7]. Several ways to interface RCs to electrodes have been described, including immobilization by Layer-by-Layer [8] and Langmuir-Blodgett [9, 10] techniques, by encapsulation in nanoporous and nanostructured materials [11-13], by entrapment in sol-gel media [8], and by employment of suitable electrode/protein linkers [14, 15]. Moreover, the efficient physisorption-based immobilization of RC by laser printing technology has been recently reported, resulting in direct photo-induced electron transfer from the working electrode to the protein [16].

Despite the huge amount of investigations driven in recent years on bio-photovoltaic devices based on immobilized RCs [6] and relevant models describing their behaviour [17-20], the scientific literature is relatively poor of reports focused on photocurrent generation by means

of photoactive proteins dissolved in the electrolyte solution [21, 22]. Photocurrent generation in these RC-based PECs occurs when RC photocycle is sustained by light in the presence of suitable electron donors and acceptors, which in turn perform the function of electron shuttles between protein and electrode surfaces. The protein acts as a photocatalyst able to promote the transfer of electrons from the donor to the acceptor, thus modifying the bulk concentrations of their different redox forms and the redox potential of the solution, according to the Nernst equation. In a three electrode system, no current flows in the external circuit if the working electrode (WE) potential is set at the open circuit potential (OCP). Nevertheless, a current will be detected at this potential under illumination as a consequence of RC-mediated equilibrium displacement. The current can be anodic or cathodic depending on the favourite reaction occurring at the WE: it is cathodic in the case of the electrochemical reduction of the donor or anodic in the case of the electrochemical oxidation of the acceptor. Setting the WE potential at a value other than OCP, the current already detected in the dark undergoes a change under light due to the photocatalytic action of the reaction centre. In this case the photocurrent is defined as the difference between light and dark currents. Of course, in such system the electrochemical reaction driven by the free energy of photons competes with the direct chemical reaction (short circuit or back reaction) between donor and acceptor, which reduces the efficiency of the photoelectrochemical device. The optimization of this RC-based transduction system requires therefore a careful evaluation of both thermodynamic and kinetic factors.

The physiological electron donor to the RC chlorophyll dimer is the water-soluble cytochrome c_2, a heme-protein having a midpoint potential of +345 mV vs NHE [23]. The mitochondrial analogue cytochrome c has been widely used in PECs with immobilized RCs [9, 10, 13, 24-27]. However, being a protein, cytochrome c suffers of the well-known disadvantages of instability and cost. Synthetic electron donors are also available, the most commonly used being the class of ferrocenes. Ferrocene itself (Fcn) has been well

characterized as an RC donor [28] and used to efficiently reduce D^+ due to its high bimolecular donation rate constant (10.1×10^6 $M^{-1}s^{-1}$) [29] and its suitable electrochemical potential ($E_m \approx +400$ mV *vs* NHE) [30]. However, the maximum pseudo first-order rate constant of electron transfer from Fcn to dimer is limited to ~ 430 s^{-1} being the water solubility of ferrocene below 80 µM [28]. With a similar midpoint potential, ferrocenemethanol (FcnMeOH) presents a different behaviour showing a lower bimolecular donation rate constant (2.1×10^6 $M^{-1}s^{-1}$) but a much higher water solubility (>1 mM). Therefore, the same donation rates achieved with Fcn can likewise be attained with FcnMeOH using suitably higher concentrations and the donation rates can be even improved further increasing the concentration.

On the other side, a number of electron acceptors can be used such as 2,3,5,6-tetramethylphenylenediamine (TMPD)[22, 31, 32] and the class of ubiquinones [29, 33-36](UQ_{10} being the physiological one). Among these, the most promising seems to be decylubiquinone (dQ), a synthetic hydrophobic quinone having a 10-carbon saturated side chain. It has been widely used as a substrate for various quinone-binding enzymes [37, 38] and recently employed for increasing mitochondrial function in synaptosomes [39].

The miniaturized photoelectrochemical transduction system described in this work is represented by a screen-printed electrochemical cell dipped in a suitable unstirred electrolyte solution where RC enzymes, extracted from *R. sphaeroides*, are dissolved. Screen-printing technology in electrochemical applications allows running a large number of electrochemical (bio-)assays at low cost. Intrinsic characteristics and reproducibility of screen-printed electrodes (SPEs) make them extremely versatile in the development of a wide range of electrochemical devices [40]. SPE-based devices containing photosynthetic proteins can find application in the sensing of herbicides and other environmental pollutants [16, 41, 42] able to inhibit selectively the photoactive component. The main advantage of using bulk-dissolved RCs in a PEC is the possibility of controlling the photocatalyst

concentration, enabling to finely modulate redox and binding reactions occurring in the aqueous homogeneous system. Hence, a theoretical model has been developed to predict the experimental photochronoamperometry profiles recorded at controlled WE potential and at variable RC concentration, allowing to obtain the concentration of all involved species as a function of time, both in the bulk and in proximity of the electrodes surface, during and after the irradiation with visible light. In this way, valuable information on the factors limiting (or enhancing) the photoresponse has been gained.

The interest of this work lies not only on the optimization of a specific transduction system for advanced sensing applications, but also in general on the elucidation of physico-chemical factors affecting the light conversion efficiency in RC-based devices, for applications in bio-photovoltaics. On the other side, the thermodynamic and kinetic properties of redox mediators, together with mass diffusion processes, discussed in this work, play a key role also in RC-based PECs where the protein is present in immobilized form.

2 Materials and methods

2.1 Chemicals

All chemicals were purchased at the highest purity available and were used without further purification. Ubiquinone-0 (UQ_0), Ubiquinone-1 (UQ_1), Ubiquinone-10 (UQ_{10}), decylubiquinone (dQ), ferrocene (Fcn), ferrocenemethanol (FcnMeOH), Triton X-100 (TX), tris(hydroxymethyl)aminomethane (Tris), diethylethanolamine (DEAE)-sephacel, ammonium sulfate, ethylenediaminetetraacetic acid (EDTA) and the reagent grade salts for the preparation of buffer solutions were purchased from Sigma. Lauryl dimethyl amino N-oxide (LDAO) was from Fluka. All aqueous solutions were prepared by using water obtained by Milli-Q Gradient A-10 system (Millipore, 18.2 MΩ cm, organic carbon content ≤4 μg/L).

2.2 Cell cultivation and RC preparation

Carotenoid-less strain *R. sphaeroides* R-26 cells were grown photoheterotrophically under anaerobic conditions in medium supplemented with potassium succinate [43].

Chromatophores and RCs were prepared as previously described [44]. RCs were solubilized by LDAO and purified by ammonium sulfate precipitation, followed by DEAE-Sephacel anion-exchange chromatography. The fractions showing OD_{280}/OD_{802} ratio below 1.4 were collected, concentrated to OD_{802} = 13, dialyzed against Tris 15 mM, EDTA 1 mM, LDAO 0.025% pH 8.0 and stored at -20°C for later use.

The aqueous medium used for photoelectrochemical measurements was K-Phosphate 10 mM, KCl 180 mM, TX 0.03% v/v, pH 7.0, I=0.2 (PBST buffer).

2.3 Electrochemical measurements

All electrochemical experiments were carried out in a three electrode configuration by means of a μStat400 portable electrochemical sensor interface workstation (DropSens, Spain) controlled by computer. Screen-printed electrodes DRP-220AT with a gold WE and relevant connectors were also from DropSens. The SPEs ceramic support is L33 x W10 x H0.5 mm; the round-shaped WE (0.12 cm^2) is partially surrounded by a silver quasi-reference electrode, while the gold counter electrode (CE) is the outermost ring of the device. The potential of the quasi-ref Ag electrode has been estimated to be +210 mV vs NHE.

The screen printed cell was immersed in a L5 x W10 x H20 mm plastic vessel filled with 0.8 mL unstirred solution. Photochronoamperometry measurements were conducted at controlled WE potential, alternating darkness and light periods. The light source was a light-emitting diode (LED) with maximum intensity centred at λ = 860 nm, with full width at half maximum of 30 nm, providing a light intensity of 25 mW/cm^2 at the surface of the WE of the electrochemical cell.

2.4 Computational analysis

The program for the simulation of photocurrent profiles, coded in Fortran 2003 and provided as supplementary material consists of a few modules, the most relevant of which are:

- dr_opt.f90, which parses the input, starts the computation and provides most of the output;
- m_dr.f90, which contains all the code pertaining the model, included the reaction kinetics and the computation of photocurrents - m_rkf.f90, a Runge-Kutta implementation with Dormand-Prince 4/5 coefficients, containing a special adaptation of step variation for chemical concentration that avoids too large relative variations;
- m_react.f90, which encodes solution of reaction rate equations for most important polynomial rate laws;
- m_diff.f90, which provides a kernel based integration of the diffusion equation with different possible contour conditions.

3 Results and discussion

3.1 Role of the applied potential

The standard electrolyte solution employed in our PEC contained FcnMeOH 300 µM, dQ 100 µM and RC 0.1 µM in PBST buffer. In such system under light the following reaction is promoted:

$$dQ + 2FcnMeOH + 2H^+ \xrightarrow{hv,RC} dQH_2 + 2FcnMeOH^+ \qquad (1).$$

The measured OCP of the cell in dark conditions was around 0.0 V *vs* quasi-ref Ag (see Fig. S1 in Supplementary Material). A series of photochronoamperometric experiments (dark-light cycles) at controlled WE potential have been conducted both at the OCP and under negative and positive overpotentials.

At the OCP, a cathodic current was detected under illumination (Fig. 1A and Fig. 1B, black trace), indicating that a reduction process at the WE is promoted by light. By applying a negative overpotential, light and dark currents (both cathodic) increased (Fig. 1A and Fig. 1B, pink and blue traces). The maximum difference between light and dark current

(photocurrent) was registered at -100 mV, although the value was very close to the one recorded at the OCP.

At +100 mV an anodic dark current was generated, whose intensity increased at +200 mV. Nevertheless, under positive overpotentials, the illumination did not induce any significant change of the dark current, which appeared only slightly perturbed by the light/dark cycles.

In order to rationalize the observed photoresponse under different WE controlled potentials, the cyclic voltammetries of the single electroactive species present in the electrolyte medium, i.e. the redox mediators, have been recorded. The cyclic voltammetry of the sole FcnMeOH, acquired in the same PBST buffer, revealed a quasi-reversible electrochemical redox transition of the couple $FcnMeOH^+$/ FcnMeOH with an experimental midpoint potential of +200 mV *vs* quasi-ref Ag (Fig. 1C, red trace). Therefore, the large anodic currents observed in the dark above +100 mV in the chronoamperometric measurements can be ascribed to FcnMeOH oxidation, while the weaker cathodic currents appearing at lower potentials arise likely from the reduction of $FcnMeOH^+$, whose concentration is expectedly low in the dark. Under illumination, the drastic enhancement of cathodic current is nicely in agreement with the increase of $FcnMeOH^+$ concentration due to its RC-mediated photogeneration. On the other hand, the cyclic voltammogram of decylubiquinone (Fig. 1C, black trace) revealed irreversible redox transitions of the dQ/dQH_2 couple at the WE surface, showing a reduction process occurring at potentials more negative than -200mV *vs* quasi-ref Ag. This finding allows excluding a role of dQ in sustaining the observed cathodic currents, nor in the dark and even less in the light. The oxidation of dQH_2 proved to occur at potentials above +100 mV. However, since the decylubiquinol is generated during the illumination step, it can contribute to sustain the anodic current, observed in the photo-chronoamperometric experiments, only under illumination, whereas its contribution to the dark anodic current is negligible. The lack of a significant enhancement of the anodic current under light, despite dQH_2 generation, can be explained with the simultaneous

depletion of reduced FcnMeOH, according to the RC photocatalytic cycle. These findings demonstrate that, under the experimental conditions employed, the gold screen printed WE functions efficiently only as photocathode. The Fig. 2 shows schematically the photoelectrochemical transduction mechanism, based on RC photocycle, accounting for the generation of cathodic photocurrents observed by applying zero or negative overpotentials.

3.2 Role of the electron donor

In absence of any donor in the electrolyte medium no cathodic photocurrent was detected, confirming that the photo-oxidized dimer is not able to withdraw electrons directly from the WE surface. Fig. 3 shows the dependence of photocurrent intensities on the concentration of FcnMeOH and Fcn at -100 mV. For both donors, a monotonic increase of the cathodic photocurrent density was observed by increasing the concentration, until a plateau was reached. For Fcn the maximum photocurrent density (around 3 $\mu A/cm^{-2}$) was reached at 80 µM, in agreement with attainment of the solubility limit. Interestingly, when FcnMeOH was employed, a plateau photocurrent of 7 $\mu A/cm^{-2}$ was registered at concentrations $\geq$ 600 µM. The achievement of a plateau in the range 600-1000 µM, where FcnMeOH is still fully soluble, demonstrates that in these conditions different parameters, other than initial donor concentration, are involved in the rate-limiting step.

3.3 Role of the electron acceptor

Looking at the acceptor side, we compared the efficiency of different quinones in sustaining the light-activated electron flow by receiving electrons at the Q_B site (Table 1). The concentration of each tested quinone has been optimized to reach the highest photocurrent. For the hydrophobic ubiquinones dQ, UQ_1 and UQ_{10} maximal photocurrents were obtained at 200 µM concentration, while for the more hydrophilic UQ_0 it was necessary to raise the concentration up to 1 mM. Unlike what happens with the donor, in this case a weak photocurrent at 0.0 V was detected even without acceptor addition, indicating that the low

amount of UQ_{10} substrate present in the RC preparation is sufficient to sustain the electron flow across the protein and mediate the electron communication with the CE. Different thermodynamic and kinetic properties account for the efficiency of quinones in wiring the RC photo-induced electron-hole pair with the electrodes. In particular, the ideal quinone acceptor must present both high affinity with the Q_B site, where the electron withdrawal from Q_A occurs, and suitable water solubility in order to shuttle rapidly electrons across the aqueous medium, also interacting with electroactive water dissolved species, such as O_2. Moreover, further factors can contribute to the different activities. For example, in our specific case, the produced quinol must not be oxidized quickly by its co-product $FcnMeOH^+$; if this short circuit reaction proceeds rapidly, the photocurrent is suppressed. The relatively low photocurrent observed with the highly soluble UQ_0 is in disagreement with a recent work by Friebe et al. [27], who reported a noteworthy activity of this electron acceptor in presence of cyt *c* as electron donor in a RC-based biophotocathode. This discrepancy is likely due to the employment of different experimental conditions, in particular the use in our work of FcnMeOH as electron donor rather than cyt *c*, which may affect the rate of UQ_0H_2 chemical oxidation. In this regard, it has been shown that UQ_0H_2 is oxidized by Fcn^+ at pH 7 with a short circuit reaction one order of magnitude faster than the one involving $UQ_{10}H_2$ [28]. The photoresponse slightly increased in the case of UQ_1, whose affinity with the Q_B site is higher. On the other hand, the natural RC substrate UQ_{10}, presenting the highest binding constant at the Q_B site, did not show the best activity, likely due to its low water solubility and its strict association to TX micelles in extra-protein environment. It is clear that dQ outperforms all tested electron acceptors, presenting the best compromise between water solubility and Q_B site affinity. A further factor in agreement with the high performances of dQ in sustaining the electron flow within our PEC is the intrinsic rate of the quinol release from the Q_B site, which has been found higher for dQ than UQ_{10} [45]. This finding has been rationalized with the enhanced flexibility of the saturated

decyl side chain of dQ whit respect to the isoprenoid one of UQ_{10}, allowing faster movements of the former once reduced [45].

3.4 Role of the photocatalyst concentration: modelling physico-chemical processes promoting photocurrent generation

A series of photochronoamperometric measurements under controlled WE potential (0.0 V *vs* quasi-ref Ag) at variable RC concentrations and constant mediators concentration (FcnMeOH 600 µM and dQ 200 µM) have been carried out. As shown in Fig. 4 (black continuous lines), the photocurrents increase with increasing the protein concentration and no saturation was observed within the concentration range investigated. With RC 3.2 µM we detected a peak photocurrent of 60 $\mu A/cm^2$. Nevertheless, a clear modification of the photochronoamperometric profile was observed, showing a progressively enhanced decay of the photocurrent following the initial rise. In order to rationalize this behaviour, gaining valuable information about the role of different processes contributing to the overall photocurrents attained, the specific features of our photo-responsive device have been examined and a simplified, yet effective, model for the simulation of [RC]-dependent chronoamperometric traces has been formulated.

Our screen printed PEC presents working and counter electrodes of comparable size, made of the same constituent material (Au) and in touch with the same electrolyte medium. These features allow assuming that: i) the CE cannot be considered an ideal non-polarizable auxiliary electrode and ii) WE and CE are expected to show the same equilibrium potential, both in dark conditions and under light, i.e. the open circuit voltage (OCV) of the cell is nominally zero. It is well known that, in a three electrode configuration, during amperometric measurements at constant WE potential, processes at the CE/solution interface cannot limit the electron flow across the cell, being the voltage between WE and CE suitably adjusted by the potentiostat. Therefore, in the photochronoamperometric measurements of

Fig. 4, the CE potential is expected to be the same as the WE (0.0 V *vs* quasi-ref Ag) at the beginning of the experiment (equilibrium dark conditions), whereas during the subsequent light/dark cycle the CE reaches a potential that is not known. Nevertheless, processes occurring at the WE, which determine the intensity of the electron flow across the cell, take place simultaneously with redox processes at the CE, that depend on the available species in solution and on their reduction potentials. It is therefore reasonable to include these processes in the modelling of our system. A schematic representation of the PEC, showing the main physico-chemical processes theoretically contributing to the photo-electrical output of the device under application of a potential equal to the dark OCP, is proposed in Fig. 5. Here, the chemical (black), electrochemical (yellow) and diffusion (red) processes involving the redox mediators are highlighted. Under light, the photochemical process 1, followed by the chemical process 2, changes the composition of the solution, with depletion of FcnMeOH and dQ and enrichment of $FcnMeOH^+$ and dQH_2, with consequent change of the Nernst potential of these redox couples. We can say that, at 0.0 V *vs* quasi-ref Ag, process 3a is favoured although process 4b may occur in some extent. We can also assume that process 3a takes place simultaneously with process 3b at the CE side, resulting in an overall electrochemical reaction (see eq. (9) later in the text) moving electrons in the external circuit in the direction of a cathodic (forward) current. On the other side, the process 4b can be considered coupled to process 4a at the CE, in agreement with an analogous electrochemical reaction this time delivering electrons in the direction of an anodic (reverse) current (see eq. (10) later in the text). Therefore, we can assume that, given the composition change induced by light, the applied potential is responsible for an unbalance between the rates of the electrochemical reactions associated to forward and reverse currents. Hence, the rate constants of these electrochemical reactions depend on the applied potential. Moreover, the asymmetry of the system under light results in the appearing of different concentration gradients at the two electrode/solution interfaces, which in turn activate diffusion processes

and affect the local rates of reactions 1 and 2. The details of the theoretical model employed for predicting the experimental traces of Fig. 4 are described in the following paragraph.

3.4.1 Model description

The model cell consisted of two parallel electrodes with a large area allowing to represent the electrolyte solution between them as a one-dimensional system, whose chemical composition can vary only along a z axis normal to the electrode surfaces (see Fig. 5). Moreover, the distance between the electrodes is much larger than the diffusion layer, enabling to apply the semi-infinite boundary conditions for mass transfer. Though the actual cell geometry is greatly different, the model geometry can be justified in consideration of two observations:

• the experiment time is about 10 s and the diffusion coefficients are certainly lower than 10^{-4} cm^2/s, therefore, according to the mean squared displacement formula ($\sqrt{\overline{z^2}} = \sqrt{2Dt}$), only a layer of solution less than 0. 5 mm thick is effectively involved in the electrode reactions;

• in the extreme case, i.e. for the largest RC concentration, the total amount of substance discharged at each electrode is about $3\ \mu A \times 10\ s\ /F \approx 3 \times 10^{-10}$ eq., that is the $FcnMeOH^+$ amount contained in 0.5 mm^3 of solution, once again the volume of a thin layer in touch with the electrode.

The large distance between the electrodes, compared to the diffusion layer, makes therefore irrelevant that the electrode surfaces are effectively parallel as in the model or not.

The z axis was divided in a suitable number of segments to ensure a good representation of the concentration variations. The electrodes are far enough to ensure that the species generated at one electrode cannot diffuse to reach the other one in the time of the experiment, i.e. part of the system is in bulk conditions. On the other side the establishment

of concentration gradients at the electrode/solution interfaces allows to identify two concentration gradient zones (see Fig.5) whose thickness varies with time.

In this space, the following processes were simulated:

A. the binding reaction between RC and dQ;
B. the redox reaction activated by light, generating dQH_2 and $FcnMeOH^+$ involving as reactant only the quinone bound to the RC;
C. the redox reaction between the photogenerated dQH_2 and $FcnMeOH^+$ (short circuit or back reaction;
D. the oxidation of dQH_2 mediated by dissolved molecular oxygen;
E. the electrochemical reactions driving the electron flow across the external circuit in both directions, according to coupling of processes 3a-3b and 4a-4b depicted in Fig.5. These processes occur at the two electrode/solution interfaces and their reaction rate provides the intensity of the electron flow, i.e. the generated current;
F. the diffusion of all the species from the electrodes to the bulk and *vice versa*, except for RC which has a uniform distribution, since it does not react at the electrodes.

Processes A, B, C and D occur everywhere in the aqueous medium, i.e. along the whole z-axis. The quinone binding reaction can be written as:

$$RC + dQ \underset{k_{out}}{\overset{k_{in}}{\rightleftarrows}} RC \cdot dQ \qquad (2),$$

where RC·dQ represents the RC-bound decylubiquinone. The RC was supposed to equilibrate with dQ very fast with a binding constant of 10^5 M [46], therefore it can be considered completely bound in most reasonable conditions. The photo-activated redox reaction, involving only RC-bound dQ molecules, is described by the following equation:

$$2FcnMeOH + RC \cdot dQ + 2H^+ \xrightarrow{h\nu} 2FcnMeOH^+ + RC \cdot dQH_2 \qquad (3).$$

The dissociation reaction of dQH_2 from the Q_B pocket:

$$RC \cdot dQH_2 \rightarrow RC + dQH_2 \qquad (4)$$

can be considered a very fast process [45], thus allowing to assume that the dQH_2 photochemical production rate (r_{ph}) depends solely on the rate of the reaction of eq. (3). For this photo-activated reaction different rate laws are possible. Keeping 1 the reaction order for RC-bound quinone, different reaction orders were tested for FcnMeOH. A value of 2 yielded to the best reproduction of experimental data, suggesting the following rate law:

$$r_{ph} = k_{ph}\left[RC \cdot dQ\right]\left[FcnMeOH\right]^2 \qquad (5)$$

The oxidation of dQH_2 by $FcnMeOH^+$ (back reaction, point C, process 2 in Fig.5), according to the chemical equation:

$$dQH_2 + 2FcnMeOH^+ \xrightarrow{k_{back}} dQ + 2FcnMeOH + 2H^+ \qquad (6),$$

provided the best agreement between simulated and experimental data for a third order rate law:

$$r_{back} = k_{back}[dQH_2][FcnMeOH^+]^2 \qquad (7).$$

Since the electrolyte medium of our experiments is aerobic, it is reasonable that dissolved oxygen plays a role in the re-oxidation of the photogenerated dQH_2. The role of dissolved oxygen in dQH_2 re-oxidation has already been highlighted in a mediator-free PEC configuration [16]. However, O_2 may support dQH_2 oxidation directly or indirectly, for instance by affecting the amount of $FcnMeOH^+$ present in the dark. Although the reaction route is expected to be rather complex, the overall rate of the processes that support dQH_2 oxidation through O_2 mediation was modelled quite simply, using a second order rate law:

$$r_{ox} = k_{ox}[dQH_2][O_2] \qquad (8).$$

As described above, the electrochemical processes can be conceived as the same dQH_2 oxidation reaction reported in equation (6), in this case occurring by shuttling the electrons across the external circuit. dQH_2 is supposed to deliver electrons both at the WE surface and at the CE surface, whilst the reduction of $FcnMeOH^+$ occurs simultaneously at the opposite electrode, according to the following processes:

$$dQH_2\,(CE) \;+\; 2FcnMeOH^+\,(WE) \xrightarrow{k_F} dQ\,(CE) \;+\; 2FcnMeOH\,(WE) \;+\; 2H^+ \qquad (9)$$

$$dQH_2\,(WE) + 2FcnMeOH^+\,(CE) \xrightarrow{k_R} dQ\,(WE) \;+\; 2FcnMeOH\,(CE) \;+\; 2H^+ \qquad (10)$$

The electrons delivered by the electrochemical process can be fed into the circuit in both directions as a direct consequence of a solubilized photocatalyst in a membrane-free configuration, which does not provide for a separation of electrode compartments [47]. The forward (i_F) and reverse (i_R) currents present opposite sign and their intensities depend on the resulting quinol oxidation rates at CE and WE respectively. A first order rate law was considered for dQH_2, whilst a second order rate law with respect $FcnMeOH^+$ allowed again the best reproduction of experimental data:

$$|i_F| \propto -\frac{d\left[dQH_2\right]^{CE}}{dt} = k_F\left[dQH_2\right]^{CE}\left(\left[FcnMeOH^+\right]^{WE}\right)^2 \qquad (11)$$

$$|i_R| \propto -\frac{d\left[dQH_2\right]^{WE}}{dt} = k_R\left[dQH_2\right]^{WE}\left(\left[FcnMeOH^+\right]^{CE}\right)^2 \qquad (12).$$

In principle, the overall current flowing in the cell i_t at a certain time depends on the relative weight of forward and reverse currents:

$$i_t = -\left(|i_F| - |i_R|\right) \qquad (13).$$

It is cathodic (negative) if the forward current overcomes the reverse one and, according to eq. (9) and eq. (10), its value is determined by the actual concentration of all involved redox species in proximity of CE and WE surfaces and by the rate constant values.

The electrochemical rate constants are strongly affected by the potential applied at the WE, in particular the ratio k_F/k_R is expected to be higher at negative overpotentials, since in these conditions the process 3a is favoured with respect to process 4b, increasing the rate of reaction of eq. (9) with respect to reaction of eq. (10).

The diffusion of the different species from and towards the electrode surfaces was modelled with the well-known second Fick law:

$$\frac{\partial C}{\partial t} = D\frac{\partial^2 C}{\partial z^2} \quad (14),$$

where C represents the concentration, D the diffusion coefficient and z the distance from the electrode. This law applies to all species except for RC whose concentration is considered uniform. Since both diffusion and reactions change the local concentrations simultaneously, any time interval was divided in 5 sub-intervals and the reactions and diffusion were allowed to occur in sequence. In this way the error due to the non-simultaneity of dynamical processes was minimized. A 6.7×10^{-6} cm^2/s diffusion coefficient in water for FcnMeOH [48] was employed in the model as a known parameter, whilst the diffusion coefficient for dQ was obtained as optimized parameter. The diffusion coefficients were considered independent on the redox state.

3.4.2 Model discussion

The simulated currents, predicting the experimental data, are shown as red broken lines in Fig. 4. Overall, the model captures the fundamental features of the experiment. In particular, the dependency on RC concentration is well reproduced. The relevant optimized parameters are listed in Table 2. The value of the diffusion coefficient of dQ was found unexpectedly three times higher than that of FcnMeOH and four times higher than that of hydrophobic quinones in a membrane bilayer (about 5×10^{-6} cm^2/s [49]). The high mobility of dQ in our micellar system can however explain the high photocurrent obtained with this quinone compared with the other tested, as shown in Table 1.

The predicted value for the O_2 concentration involved in dQH_2 oxidation was 51 µM, which represents only a fraction of the expected dissolved oxygen concentration in the experimental conditions employed. Although our model requires this contribution for the effective simulation of the experimental data, the rate r_{ox}, given by eq. (8), drops to zero in the very first moments of the light period, after which the electron withdrawal from dQH_2,

both in the electrolyte medium (back reaction) and via the external circuit (electrode reactions), proceeds only by means of photo-generated $FcnMeOH^+$.

The rate constant k_{back} arising from the model corresponds to a pseudo-second order rate constant of $\approx 7\times10^4$ $M^{-1}s^{-1}$, in good agreement with a previous estimation of $\approx 2\ 10^4 M^{-1}s^{-1}$ [29]. The computational procedure of parameter optimization led to $k_F/k_R \approx 10$, in agreement with favoured cathodic processes at the WE.

Upper and middle panels in Fig. 6 show the time course of dQH_2 and $FcnMeOH^+$ concentration at the WE surface, at the CE surface and far from the electrodes. In the bulk dQH_2 and $FcnMeOH^+$ rapidly reach a steady value which depends on the balance between dQH_2 photogeneration and its consumption due to the back reaction. As expected, such steady values increase with RC concentration, as photogeneration becomes faster ([RC·dQ] increases). However, even at the highest RC concentration tested, the percentage of FcnMeOH converted in $FcnMeOH^+$ at the steady state is 32% and the percentage of dQ converted in dQH_2 is 35%. This finding highlights the major role played by the back reaction in counteracting the chemical composition change induced by light.

The time course of the intensity of virtual currents generated by forward and reverse electrochemical processes for the case of [RC]=3.2 μM is shown in Fig. 7, together with the resulting overall current, whose intensity profile nicely reproduces the experimental one. As expected, both forward and reverse current intensities are larger than the resulting one and a maximum difference between them is observed at 0.8 s, where the experimental current presents a characteristic peak. In general, the electrode reactions produce the depletion of dQH_2 and $FcnMeOH^+$ at both the electrode/solution interfaces and the simultaneous release of dQ and FcnMeOH. These changes of concentration with respect to the bulk activate the gradient-driven diffusion processes and affect the rate of the photochemical and back reactions in proximity of the electrodes, according to the relevant rate laws. In the presence of an applied WE potential, inducing asymmetry of the system ($k_F/k_R \neq 1$) and the subsequent

current generation, the depletion/release of reactant/product species at the electrode/solution interfaces occur at different rates. In particular, at 0.0 V applied potential, the decrease under light of $FcnMeOH^+$ concentration is more pronounced at the WE than at the CE. The back reaction thus undergoes an efficiency drop more enhanced in proximity of the WE, according to eq. (7), causing the local accumulation of dQH_2. Despite its consumption due to the reverse electrochemical reaction, the concentration of this species can indeed attain at the WE values even higher than in the bulk (see Fig. 6, upper panels). It should be mentioned that the photochemical reaction rate near the WE is poorly influenced by the electrochemical reaction process, since the regeneration of the reactant FcnMeOH is however guaranteed and the concentration of RC·dQ remains basically constant. Upon light switching off, the sudden stop of dQH_2 and $FcnMeOH^+$ photo-production causes the drastic decrease of both reverse and forward currents. Nevertheless, the reduced efficiency of the back reaction at the WE allows here the attenuation of dQH_2 concentration drop, which in turn results in a slower collapse of the reverse current with respect to the forward one (see Fig. 7). This effect is responsible for the characteristic current inversion observed at RC concentrations above 0.8 µM during the dark phase following the illumination interval (Fig. 4).

As expected, since the z axis points from the CE towards the WE, the dQH_2 gradients at the two electrode/solution interfaces (Fig 7, lower panel) present opposite sign. However the curves describing their time evolution are not symmetrical because higher gradients appear at the CE/solution interface. This is likely a consequence of enhanced dQH_2 consumption at the CE due to the higher rate of the electrochemical forward reaction. After the initial instability, the gradients become constant as soon as dQH_2 and FcnMeOH concentrations reach a steady value in the bulk.

The concentration profiles of dQH_2 and $FcnMeOH^+$ along the z-axis at different representative times are depicted in Fig. 8. Here the effect of the electrochemical processes on the back reaction rate is further highlighted. It is clear that both dQH_2 and $FcnMeOH^+$

accumulate at opposite electrodes reaching concentration values higher than in the bulk. The electrochemical $FcnMeOH^+$ depletion at the WE induces the accumulation of dQH_2 as a consequence of back reaction slowing down, whereas, for the same reason, the electrochemical depletion of dQH_2 at the CE induces here the accumulation of $FcnMeOH^+$. An important factor accounting for the appearing of characteristic concentration peaks at a small distance from the electrode surface is the diffusion of the species involved. The slow mass transport prevents indeed the rapid re-equilibration of the system composition perturbed by the electrode processes, thus allowing the chemical reaction rates to be significantly affected by local concentration changes. In the time of the experiment, the thickness of the solution layer in which fluctuations of dQH_2 and $FcnMeOH^+$ concentration appear is ~0.4 mm. The green traces in Fig. 8 show the spatial distribution of these species after stopping the photochemical reaction. As expected, an overall concentration drop occurs. The shape of the [$FcnMeOH^+$] profile is however conserved, while negative [dQH_2] gradients at the electrode interfaces appear, especially at high RC concentration. In the dark, far from the electrode surface, only the chemical dQH_2 oxidation by $FcnMeOH^+$ takes place, therefore the inhomogeneity of [dQH_2] and [$FcnMeOH^+$] profile reflects the inhomogeneity of the back reaction rate along the z-axis.

4 Conclusions

A photoelectrochemical cell based on solubilized reaction centres from the phototrophic bacterium *Rhodobacter sphaeroides* has been designed and characterized. Our miniaturized non-stirred SPE-based bio-hybrid device allows the generation of high S/N photocurrents with plateau intensities reaching 15 $\mu A/cm^2$. The high solubility of FcnMeOH and its suitable redox potential, together with the optimal thermodynamic and kinetic properties of dQ, allowed to maximize the device photoresponse. The relative amounts of donor, acceptor and RC affect the intensity of photocurrents as well as the chronoamperometric profiles.

More intense photocurrents can be generated at higher RC concentrations, although in this case the profile becomes less regular, showing a fast current rise until a peak value, followed by a slower decay.

The simulation of electrochemical, chemical, photochemical and diffusion processes, taking place simultaneously in the cell, allowed the calculation of physico-chemical parameters that shed light on the mechanisms that govern generation and time course of photocurrents promoted by photosynthetic proteins solubilized in the electrolyte medium, in the presence of redox mediators. Our model, describing the electrode processes with the same rate laws of homogeneous chemical reactions, proved to be very effective in predicting the electrical output of the cell both under light and in the dark phase immediately following the illumination. Interestingly, even the peculiar current inversion (from cathodic to anodic), observed in the post-light period at high RC concentrations, was well described by the model and can be rationalized on the basis of an imbalance between forward and reverse currents in favour of the latter one. Moreover, the model highlighted nicely the role of the short-circuit chemical reaction (back reaction) that, not only represents the main factor lowering the light/electricity conversion yield, but also affects significantly the shape of the chronoamperometric profile. The back reaction was found to proceed at a specific rate slightly lower than the photochemical one and accounts for the fast current drop upon light switching off. Our results demonstrate that the regeneration of redox mediators reacting at the electrodes by means of the RC-catalysed photochemical reaction is not sufficient to sustain a steady photocurrent. The electrochemical reactions induce indeed chemical composition changes at the electrode/solution interfaces that in turn affect chemical reaction rates. The resulting time-dependent concentration profiles, establishing near the electrodes, are therefore the outcome of chemical and mass transport processes occurring simultaneously.

This investigation represents a further contribution to the comprehension of factors that regulate light energy conversion in protein-based and bio-inspired photoelectrochemical devices. On the other side, the generated photocurrents represent a good physical observable for the selective detection of herbicides and specific environmental pollutants, able to inhibit the reaction centre photoactivity. From this applicative point of view, a herbicide biosensing system based on the photo-transducer here described, would be not only very easy to assemble and to handle, since no protein immobilization step is required, but also competitive for cheapness and versatility due to the employment of SPE technology.

Acknowledgements

This work was financially supported by Ministero dell'Istruzione, dell'Università e della Ricerca (MIUR), Research Project of National Interest (prot. 2010C4R8M8); MIUR and DiTECH (PON 02_00563_3316357 Molecular Nanotechnology for Health and Environment MAAT).

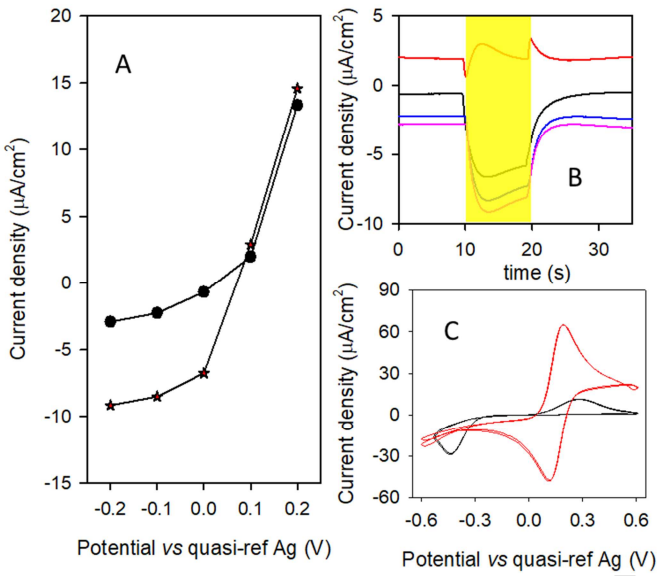

Figure 1. (A) Peak currents detected in the dark (circles) and under illumination (stars) as a function of the applied potential, using an Au WE, with RC 0.1 µM, dQ 100 µM, FcnMeOH 300 µM. (B) Photocurrent profile recorded at -200 mV (pink), -100 mV (blue), 0 mV (black) and +100 mV (red) *vs* quasi-ref Ag, the illumination period is highlighted in yellow. (C) Cyclic voltammetry of FcnMeOH 300 µM (red) and dQ 100 µM (black) in PBST buffer at +100 mVs^{-1}, after subtraction of the baseline.

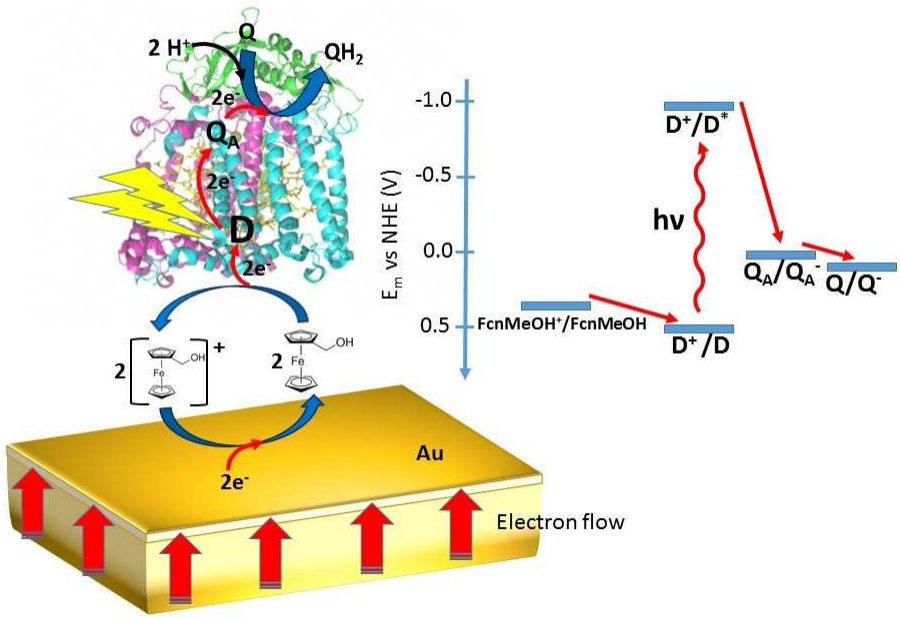

Figure 2. Mechanism of cathodic photocurrent generation with FcnMeOH shuttling electrons from the WE to the photo-oxidized RC dimer (D). Q_A represents UQ_{10} firmly bound to the Q_A site. Q represents a generic quinone acceptor that binds to the Q_B site, leaving the same site as a quinol (QH_2) molecule, after double reduction and protonation. The energy diagram on the right depicts the spontaneous electron transfers activated by light-absorption.

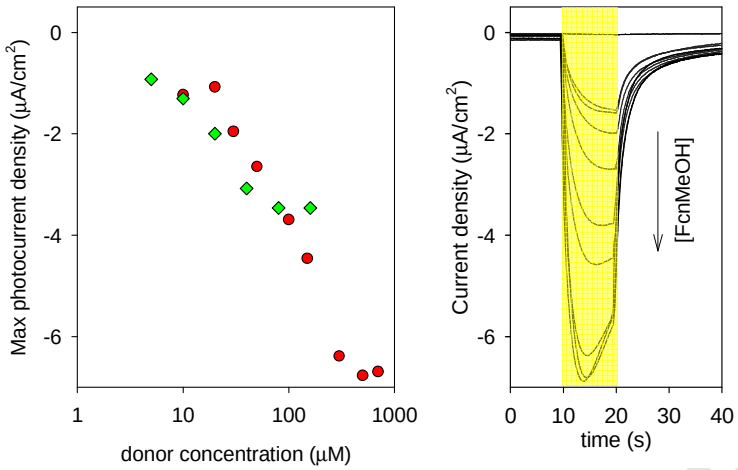

Figure 3. (Left) Intensity of cathodic photocurrents (peak values) detected with a gold WE at the dark OCP (0.0 V vs quasi-ref Ag) as a function of FcnMeOH (red circles) and Fcn (green diamonds) concentration, with RC 0.1 µM and dQ 50 µM in PBST buffer. (Right) Relevant current profiles for the same FcnMeOH concentrations reported in the graph on the left. The illumination period is highlighted in yellow.

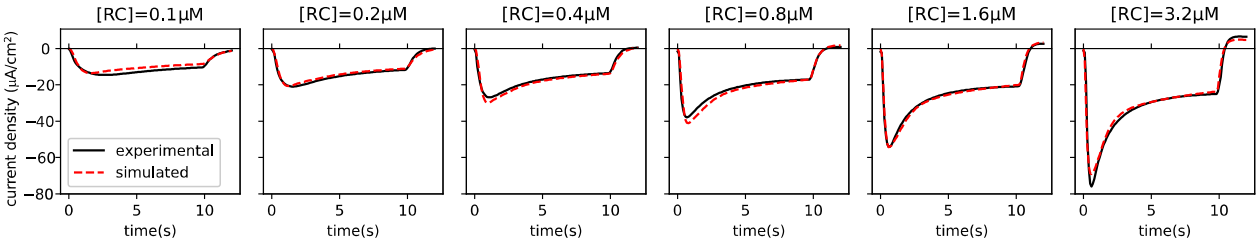

Figure 4. Experimental (black continuous lines) and predicted (red broken lines) photochronoamperometric traces at controlled WE potential (0.0 V vs quasi-ref Ag) detected or calculated with RC variable from 0.1 to 3.2 µM in presence of FcnMeOH 600 µM and dQ 200 µM. The illumination starts at 0 s and ends at 10 s.

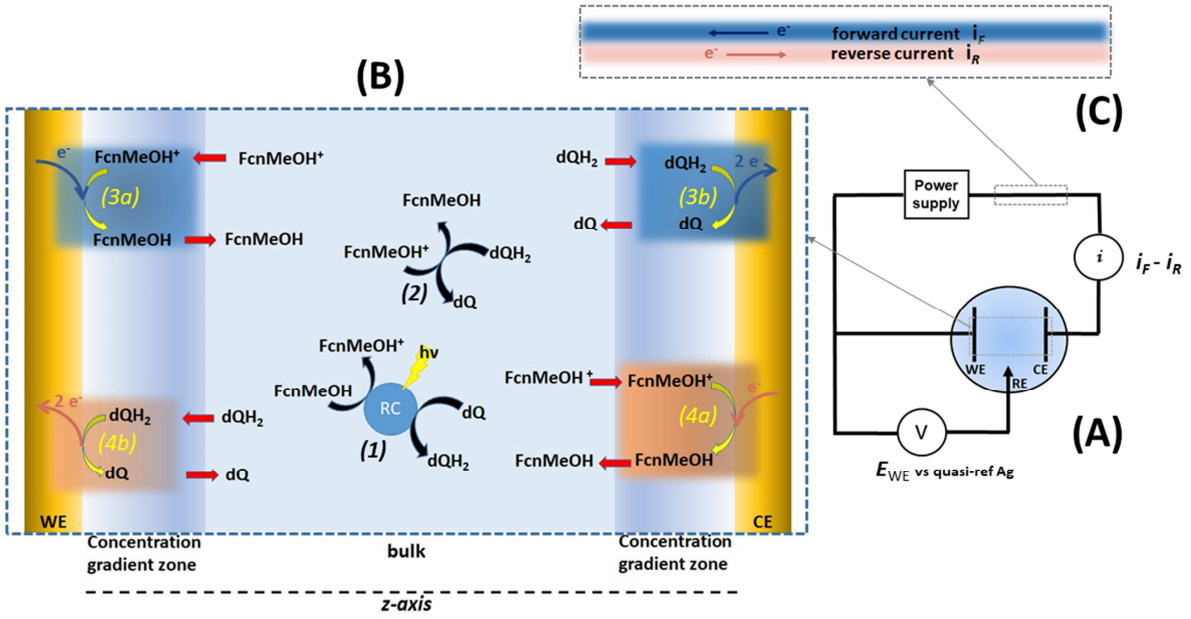

Figure 5. Schematic representation of the electrochemical cell in the three electrode configuration (A), with a focus on the electrolyte space between WE and CE (B) where the physico-chemical processes responsible for the photocurrent generation take place. The black arrows depict the redox transitions of the mediators due to photochemical (1) and chemical (2) processes. Although represented in the bulk phase, these processes occur in the whole solution, both in the bulk and in the concentration gradient zones. The yellow arrows indicate the redox transitions of the mediators due to electrochemical processes (half-reactions). The protons and the right stoichiometry of chemical processes are omitted. Diffusion processes to/from the electrode surfaces are denoted by red arrows. The overall electrochemical processes resulting from the sum of blue coloured (3a-3b) and orange coloured (4a-4b) half reactions move electrons in the external circuit in the direction (forward and reverse, respectively) depicted in (C).

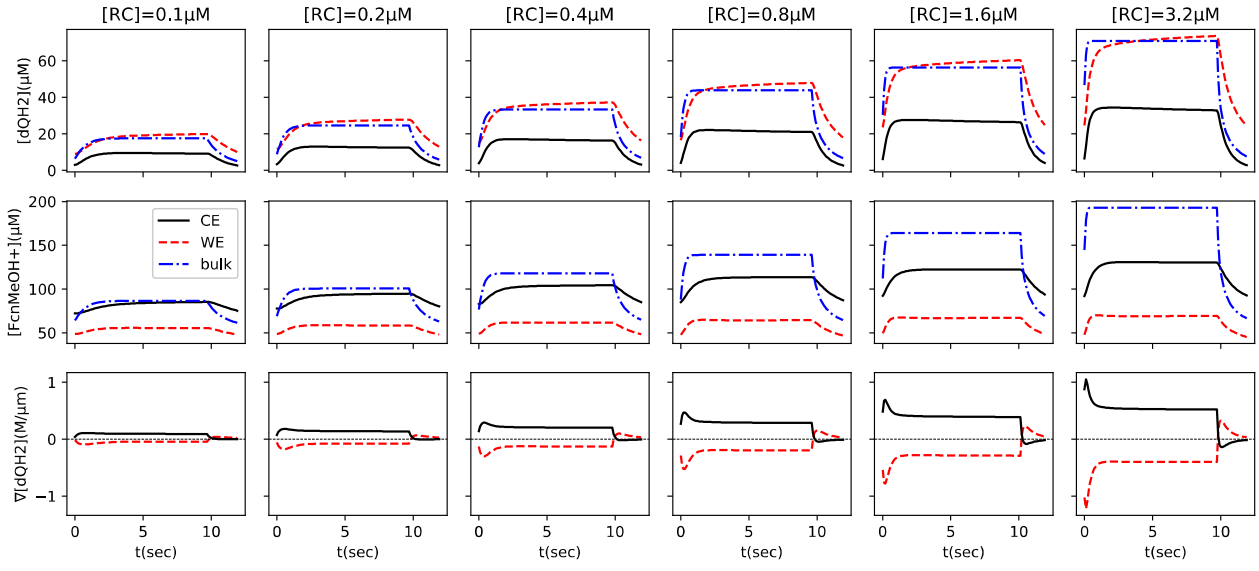

Figure 6. Predicted concentrations of dQH_2 (upper panel) and $FcnMeOH^+$ (middle panel) at different times during the photocurrent generation experiments illustrated in Fig. 4 and in different points along the z-axis: at the WE surface (red dashed lines), at the CE surface (black lines) and far from the electrodes (blue broken lines). Lower panels represent the time course of dQH_2 concentration gradients at the WE (red dashed lines) and CE (black lines) surface. The illumination starts at 0 s and ends at 10 s.

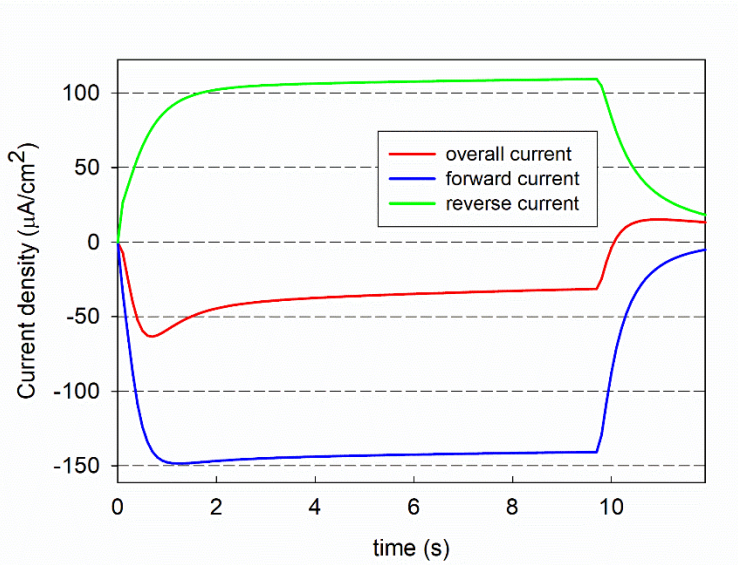

Figure 7. Time course of the intensity of forward (blue) and reverse (green) virtual currents as arising from the computational simulation for the case of [RC]=3.2 µM, [FcnMeOH]=600 µM, [dQ]=200 µM, WE applied potential=0.0 V *vs* quasi-ref Ag . The red trace represents the predicted current profile, obtained as the difference between forward and reverse currents (see eq. 13 in the text).

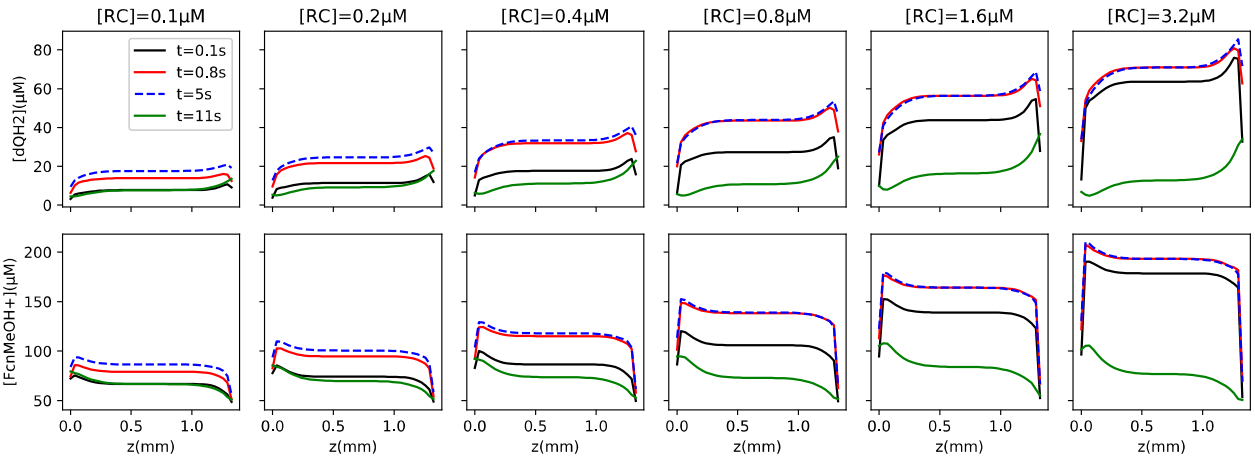

Figure 8. Concentration of dQH_2 (upper panel) and $FcnMeOH^+$ (lower panel) as a function of the distance from the electrode surfaces at different representative times: 0.1 s (black), 0.8 s (red), 5 s (blue), 11 s (green), relevant to the photocurrent generation experiments illustrated in Fig. 4. The CE surface is at z=0 (left) and the WE surface is at $z=z_{max}$ (right). Since the length of the z axis is arbitrary, the thickness of the bulk region has been reduced in order to emphasize the concentration variations near the electrodes.

Table 1. Optimal concentrations and relevant peak photocurrent densities detected at 0.0 mV *vs* quasi-ref Ag for different quinone acceptors with RC 0.1 µM and FcnMeOH 300 µM in PBST buffer. The value detected with no added electron acceptor is also reported for comparison.

Quinone	Optimal concentration (mM)	Peak photocurrent density ($\mu A/cm^2$)
-	-	0.3
dQ	0.20	6.8
UQ_{10}	0.20	3.6
UQ_1	0.20	1.1
UQ_0	1.00	1.3

Table 2. Optimized parameters arising from simulation of the photochronoamperometric profiles at variable RC concentration.

Parameter		Optimized value
D_{dQ}	Diffusion coefficient of dQ	19.6×10^{-6} cm^2s^{-1}
k_{ph}	Rate constant of light activated reaction (eq. 5)	5.71×10^{8} $M^{-2}s^{-1}$
k_{back}	Rate constant of short circuit dQH_2 oxidation (eq. 7)	1.15×10^{8} $M^{-2}s^{-1}$
$[O_2]_0$	Concentration of O_2 involved in dQH_2 oxidation	51.3 µM
k_{ox}	Rate constant of dQH_2 oxidation through O_2 mediation (eq. 8)	2.27×10^{4} $M^{-1}s^{-1}$
k_F	Rate constant of forward electrochemical reaction (eq. 11)	2.40×10^{8} $M^{-2}s^{-1}$
k_R	Rate constant of reverse electrochemical reaction (eq. 12)	2.37×10^{7} $M^{-2}s^{-1}$

References

[1] J.P. Allen, J.C. Williams, Photosynthetic reaction centers, FEBS Lett., 438 (1998) 5-9.
[2] L. Nagy, M. Magyar, T. Szabo, K. Hajdu, L. Giotta, M. Dorogi, F. Milano, Photosynthetic Machineries in Nano-Systems, Curr. Protein Peptide Sci., 15 (2014) 363-373.
[3] K. Hajdu, T. Szabo, A. Sarrai, L. Rinyu, L. Nagy, Functional Nanohybrid Materials from Photosynthetic Reaction Center Proteins, International Journal of Photoenergy, (2017) 14.
[4] V.M. Friebe, R.N. Frese, Photosynthetic reaction center-based biophotovoltaics, Current Opinion in Electrochemistry, 5 (2017) 126-134.
[5] D.J. Swainsbury, V.M. Friebe, R.N. Frese, M.R. Jones, Evaluation of a biohybrid photoelectrochemical cell employing the purple bacterial reaction centre as a biosensor for herbicides, Biosens. Bioelectron., 58 (2014) 172-178.
[6] S.K. Ravi, S.C. Tan, Progress and perspectives in exploiting photosynthetic biomolecules for solar energy harnessing, Energy Environ. Sci., 8 (2015) 2551-2573.
[7] O. Yehezkeli, R. Tel-Vered, D. Michaeli, I. Willner, R. Nechushtai, Photosynthetic reaction center-functionalized electrodes for photo-bioelectrochemical cells, Photosynth. Res., (2013).

[8] J. Zhao, B. Liu, Y. Zou, C. Xu, J. Kong, Photoelectric conversion of photosynthetic reaction center in multilayered films fabricated by layer-by-layer assembly, Electrochim. Acta, 47 (2002) 2013-2017.
[9] M. Kamran, J.D. Delgado, V. Friebe, T.J. Aartsma, R.N. Frese, Photosynthetic protein complexes as bio-photovoltaic building blocks retaining a high internal quantum efficiency, Biomacromolecules, 15 (2014) 2833-2838.
[10] M. Kamran, V.M. Friebe, J.D. Delgado, T.J. Aartsma, R.N. Frese, M.R. Jones, Demonstration of asymmetric electron conduction in pseudosymmetrical photosynthetic reaction centre proteins in an electrical circuit, Nature Communications, 6 (2015) 6530-6539.
[11] K. Hajdu, C. Gergely, M. Martin, T. Cloitre, L. Zimanyi, K. Tenger, P. Khoroshyy, G. Palestino, V. Agarwal, K. Hernadi, Z. Nemeth, L. Nagy, Porous Silicon/Photosynthetic Reaction Center Hybrid Nanostructure, Langmuir, 28 (2012) 11866-11873.
[12] I. Oda, M. Iwaki, D. Fujita, Y. Tsutsui, S. Ishizaka, M. Dewa, M. Nango, T. Kajino, Y. Fukushima, S. Itoh, Photosynthetic Electron Transfer from Reaction Center Pigment-Protein Complex in Silica Nanopores, Langmuir, 26 (2010) 13399-13406.
[13] N. Lebedev, S.A. Trammell, S. Tsoi, A. Spano, J.H. Kim, J. Xu, M.E. Twigg, J.M. Schnur, Increasing efficiency of photoelectronic conversion by encapsulation of photosynthetic reaction center proteins in arrayed carbon nanotube electrode, Langmuir, 24 (2008) 8871-8876.
[14] J. Gebert, C. Reiner-Rozman, C. Steininger, V. Nedelkovski, C. Nowak, C.A. Wraight, R.L.C. Naumann, Electron Transfer to Light-Activated Photosynthetic Reaction Centers from Rhodobacter sphaeroides Reconstituted in a Biomimetic Membrane System, J. Phys. Chem. C, 119 (2015) 890-895.
[15] M. Kondo, K. Iida, T. Dewa, H. Tanaka, T. Ogawa, S. Nagashima, K.V.P. Nagashima, K. Shimada, H. Hashimoto, A.T. Gardiner, R.J. Cogdell, M. Nango, Photocurrent and Electronic Activities of Oriented-His-Tagged Photosynthetic Light-Harvesting/Reaction Center Core Complexes Assembled onto a Gold Electrode, Biomacromolecules, 13 (2012) 432-438.
[16] M. Chatzipetrou, F. Milano, L. Giotta, D. Chirizzi, M. Trotta, M. Massaouti, M.R. Guascito, I. Zergioti, Functionalization of gold screen printed electrodes with bacterial photosynthetic reaction centers by laser printing technology for mediatorless herbicide biosensing, Electrochem. Commun., 64 (2016) 46-50.
[17] R. Caterino, R. Csiki, A. Lyuleeva, J. Pfisterer, M. Wiesinger, S.D. Janssens, K. Haenen, A. Cattani-Scholz, M. Stutzmann, J.A. Garrido, Photocurrent generation in diamond electrodes modified with reaction centers, ACS Appl. Mater. Interfaces, 7 (2015) 8099-8107.
[18] A. Takshi, J.D. Madden, J.T. Beatty, Diffusion model for charge transfer from a photosynthetic reaction center to an electrode in a photovoltaic device, Electrochim. Acta, 54 (2009) 3806-3811.
[19] M.T. Robinson, D.E. Cliffel, G.K. Jennings, An Electrochemical Reaction-Diffusion Model of the Photocatalytic Effect of Photosystem I Multilayer Films, The Journal of Physical Chemistry B, 122 (2018) 117-125.
[20] P.N. Ciesielski, D.E. Cliffel, G.K. Jennings, Kinetic Model of the Photocatalytic Effect of a Photosystem I Monolayer on a Planar Electrode Surface, The Journal of Physical Chemistry A, 115 (2011) 3326-3334.
[21] A. Takshi, J.D.W. Madden, A. Mahmoudzadeh, R. Saer, J.T. Beatty, A Photovoltaic Device Using an Electrolyte Containing Photosynthetic Reaction Centers, Energies, 3 (2010) 1721-1727.
[22] S.C. Tan, L.I. Crouch, M.R. Jones, M. Welland, Generation of alternating current in response to discontinuous illumination by photoelectrochemical cells based on photosynthetic proteins, Angew. Chem. Int. Ed. Engl., 51 (2012) 6667-6671.
[23] J.R. Bowyer, S.W. Meinhardt, G.V. Tierney, A.R. Crofts, Resolved difference spectra of redox centers involved in photosynthetic electron flow in Rhodopseudomonas capsulata and Rhodopseudomonas sphaeroides, Biochim. Biophys. Acta, 635 (1981) 167-186.
[24] S.A. Trammell, A. Spano, R. Price, N. Lebedev, Effect of protein orientation on electron transfer between photosynthetic reaction centers and carbon electrodes, Biosens. Bioelectron., 21 (2006) 1023-1028.
[25] H. Yaghoubi, Z. Li, D. Jun, R. Saer, J.E. Slota, M. Beerbom, R. Schlaf, J.D. Madden, J.T. Beatty, A. Takshi, The Role of Gold-Adsorbed Photosynthetic Reaction Centers and Redox Mediators in the Charge Transfer and Photocurrent Generation in a Bio-Photoelectrochemical Cell, The Journal of Physical Chemistry C, 116 (2012) 24868-24877.
[26] T. Noji, M. Matsuo, N. Takeda, A. Sumino, M. Kondo, M. Nango, S. Itoh, T. Dewa, Lipid-Controlled Stabilization of Charge-Separated States (P+QB–) and Photocurrent Generation Activity of a Light-Harvesting–Reaction Center Core Complex (LH1-RC) from Rhodopseudomonas palustris, The Journal of Physical Chemistry B, 122 (2018) 1066-1080.
[27] V.M. Friebe, D. Millo, D.J.K. Swainsbury, M.R. Jones, R.N. Frese, Cytochrome c Provides an Electron-Funneling Antenna for Efficient Photocurrent Generation in a Reaction Center Biophotocathode, ACS Applied Materials & Interfaces, 9 (2017) 23379-23388.

[28] F. Milano, L. Gerencser, A. Agostiano, L. Nagy, M. Trotta, P. Maroti, Mechanism of quinol oxidation by ferricenium produced by light excitation in reaction centers of photosynthetic bacteria, J. Phys. Chem. B, 111 (2007) 4261-4270.
[29] F. Ciriaco, R.R. Tangorra, A. Antonucci, L. Giotta, A. Agostiano, M. Trotta, F. Milano, Semiquinone oscillations as a tool for investigating the ubiquinone binding to photosynthetic reaction centers, Eur. Biophys. J., 44 (2015) 183-192.
[30] J. Georges, S. Desmettre, Electrochemistry of ferrocene in anionic, cationic and nonionic micellar solutions. Effet of the micelle solubilization of the half-wave potentials, Electrochim. Acta, 29 (1984) 521-525.
[31] S.C. Tan, F. Yan, L.I. Crouch, J. Robertson, M.R. Jones, M.E. Welland, Superhydrophobic Carbon Nanotube Electrode Produces a Near-Symmetrical Alternating Current from Photosynthetic Protein-Based Photoelectrochemical Cells, Adv. Funct. Mater., 23 (2013) 5556-5563.
[32] S.K. Ravi, Z. Yu, D.J.K. Swainsbury, J. Ouyang, M.R. Jones, S.C. Tan, Enhanced Output from Biohybrid Photoelectrochemical Transparent Tandem Cells Integrating Photosynthetic Proteins Genetically Modified for Expanded Solar Energy Harvesting, Advanced Energy Materials, 7 (2017) 1601821.
[33] D.A. Moss, M. Leonhard, M. Bauscher, W. Mantele, Electrochemical redox titration of cofactors in the reaction center from Rhodobacter sphaeroides, FEBS Lett., 283 (1991) 33-36.
[34] E.Y. Katz, A.Y. Shkuropatov, V.A. Shuvalov, Electrochemical approach to the development of a photoelectrode on the basis of photosynthetic reaction centers, Bioelectrochem. Bioenerget., 23 (1990) 239-247.
[35] A.M. Carey, H.J. Zhang, M.H. Liu, D. Sharaf, N. Akram, H. Yan, S. Lin, N.W. Woodbury, D.K. Seo, Enhancing Photocurrent Generation in Photosynthetic Reaction Center-Based Photoelectrochemical Cells with Biomimetic DNA Antenna, Chemsuschem, 10 (2017) 4457-4460.
[36] V.M. Friebe, D.J.K. Swainsbury, P.K. Fyfe, W. van der Heijden, M.R. Jones, R.N. Frese, On the mechanism of ubiquinone mediated photocurrent generation by a reaction center based photocathode, Biochimica Et Biophysica Acta-Bioenergetics, 1857 (2016) 1925-1934.
[37] A. Graff, C. Fraysse-Ailhas, C.G. Palivan, M. Grzelakowski, T. Friedrich, C. Vebert, G. Gescheidt, W. Meier, Amphiphilic Copolymer Membranes Promote NADH:Ubiquinone Oxidoreductase Activity: Towards an Electron-Transfer Nanodevice, Macromol. Chem. Phys., 211 (2010) 229-238.
[38] R.R. Tangorra, A. Operamolla, F. Milano, O. Hassan Omar, J. Henrard, R. Comparelli, F. Italiano, A. Agostiano, V. De Leo, R. Marotta, A. Falqui, G.M. Farinola, M. Trotta, Assembly of a photosynthetic reaction center with ABA tri-block polymersomes: highlights on protein localization, Photochem. Photobiol. Sci., 14 (2015) 1844-1852.
[39] J.E. Telford, S.M. Kilbride, G.P. Davey, Decylubiquinone increases mitochondrial function in synaptosomes, J. Biol. Chem., 285 (2010) 8639-8645.
[40] M. Li, Y.-T. Li, D.-W. Li, Y.-T. Long, Recent developments and applications of screen-printed electrodes in environmental assays—A review, Anal. Chim. Acta, 734 (2012) 31-44.
[41] E. Touloupakis, S.A. Giannoudi L Fau - Piletsky, L. Piletsky Sa Fau - Guzzella, F. Guzzella L Fau - Pozzoni, M.T. Pozzoni F Fau - Giardi, M.T. Giardi, A multi-biosensor based on immobilized Photosystem II on screen-printed electrodes for the detection of herbicides in river water.
[42] V. Bhalla, V. Zazubovich, Self-assembly and sensor response of photosynthetic reaction centers on screen-printed electrodes, Anal. Chim. Acta, 707 (2011) 184-190.
[43] L. Giotta, A. Agostiano, F. Italiano, F. Milano, M. Trotta, Heavy metal ion influence on the photosynthetic growth of Rhodobacter sphaeroides, Chemosphere, 62 (2006) 1490-1499.
[44] R.A. Isaacson, F. Lendzian, E.C. Abresch, W. Lubitz, G. Feher, Electronic structure of Q-A in reaction centers from Rhodobacter sphaeroides. I. Electron paramagnetic resonance in single crystals, Biophys. J., 69 (1995) 311-322.
[45] O.A. Gopta, A.Y. Semenov, D.A. Bloch, Electrogenic proton transfer in Rhodobacter sphaeroides reaction centers: effect of coenzyme Q(10) substitution by decylubiquinone in the Q(B) binding site, FEBS Lett., 499 (2001) 116-120.
[46] J.C. McComb, R.R. Stein, C.A. Wraight, Investigations on the influence of headgroup substitution and isoprene side-chain length in the function of primary and secondary quinones of bacterial reaction centers, Biochim. Biophys. Acta, 1015 (1990) 156-171.
[47] B. Yan, N.M. Concannon, J.D. Milshtein, F.R. Brushett, Y.A.-O.h.o.o. Surendranath, A Membrane-Free Neutral pH Formate Fuel Cell Enabled by a Selective Nickel Sulfide Oxygen Reduction Catalyst.
[48] N. Anicet, C. Bourdillon, J. Moiroux, J.-M. Savéant, Electron Transfer in Organized Assemblies of Biomolecules. Step-by-Step Avidin/Biotin Construction and Dynamic Characteristics of a Spatially Ordered Multilayer Enzyme Electrode, The Journal of Physical Chemistry B, 102 (1998) 9844-9849.

[49] R. Fato, M. Battino, M. Degli-Esposti, G. Parenti-Castelli, G. Lenaz, Determination of partition and lateral diffusion coefficients of ubiquinones by fluorescence quenching of N-(9-anthroyloxy)stearic acids in phospholipid vesicles and mitochondrial mambranes, Biochemistry, 25 (1986) 3378-3390.

Highlights

- A photoelectrochemical transduction system based on solubilised RCs is presented
- Ferrocenemethanol and decylubiquinone act as efficient redox mediators for RC wiring
- The WE acts as photocathode by applying the OCP measured in the dark
- The intensity and the time course of the photocurrent depend on the RC concentration
- The photochronoamperometric profiles are predicted by a suitable computational model